Higher Josephson Harmonics in a Tunable Double-Junction Transmon Qubit

Ksenia Shagalov,[1,2,*] David Feldstein-Bofill,[1,2] Leo Uhre Jakobsen,[1,2] Zhenhai Sun,[1,2] Casper Wied,[1,2] Amalie T. J. Paulsen,[1,2] Johann Bock Severin,[1,2] Malthe A. Marciniak,[1,2] Clinton A. Potts,[1,2,3] Anders Kringhøj,[1,2] Jacob Hastrup,[1,2] Karsten Flensberg,[1] Svend Krøjer,[1,2] and Morten Kjaergaard[1,2,†]

[1]*Center for Quantum Devices, Niels Bohr Institute, University of Copenhagen, 2100 Copenhagen, Denmark*

[2]*NNF Quantum Computing Programme, Niels Bohr Institute, University of Copenhagen, 2100 Copenhagen, Denmark*

[3]*Department of Electrical and Software Engineering, University of Calgary, 2500 University Drive NW, Calgary, Alberta T2N 1N4, Canada*

(Received 20 December 2025; accepted 26 June 2026; published 28 July 2026)

Tunable Josephson harmonics open new avenues for qubit design. We demonstrate a superconducting circuit element consisting of a tunnel junction in series with a superconducting quantum interference device (SQUID) loop, yielding a Josephson potential whose harmonic content is strongly tunable by magnetic flux. Through spectroscopy of the first four qubit transitions, together with an effective single-mode model renormalized by the internal mode, we resolve a second harmonic with an amplitude up to ∼10% of the fundamental. We identify a flux sweet spot where the ground-state dispersive shift vanishes, achieved by balancing the dispersive couplings to the internal and qubit modes. This highly tunable element provides a route toward protected qubits and customizable nonlinear microwave devices.

DOI: 10.1103/fr7x-555s

Superconductor-insulator-superconductor (SIS) Josephson junctions (JJs) form the nonlinear element in most superconducting circuits [1]. The corresponding Josephson potential is conventionally modeled by a single harmonic, $U(\phi) = -E_J \cos\phi$, with E_J being Josephson energy [2], which underpins key circuit properties, including anharmonicity and charge-noise sensitivity. However, recent experiments have shown that SIS junctions can exhibit higher harmonics, i.e., terms proportional to $\cos(k\phi)$ with $k > 1$, arising from pinholes in the junction or from inductive contributions of the leads [3–6].

Generalizing these observations, the potential of a superconducting Josephson element can be described through a Fourier series,

$$U(\phi) = \sum_{k=1}^{\infty} U_k \cos(k\phi), \tag{1}$$

where U_k are the harmonic coefficients with the kth term corresponding to transmission of k pairs of Cooper pairs across the junction [7]. Controlling the ratio between the first and higher Josephson harmonics, thus, enables modifications of the potential energy landscape of a superconducting circuit. Importantly, higher harmonic engineering has enabled the design of protected qubits with suppressed sensitivity to charge or flux noise [8–15] and superconducting diodes [16–19].

One approach toward generating higher Josephson harmonics uses superconductor-normal metal-superconductor (SNS) junctions [20] and hybrid superconductor-semiconductor weak links [21]. In SNS elements, multiple Andreev reflections enable multi-Cooper-pair tunneling, producing a strongly nonsinusoidal potential [22] with a substantially higher harmonic content [9,23,24]. Such junctions have been used to demonstrate gate-tunable qubits [25–27], Φ_0 junctions [28], and diodelike behavior [16–19]. However, hybrid platforms often suffer from frequency instability and reduced coherence, potentially due to losses in the semiconducting region [29,30].

Another approach relies on placing two SIS junctions in series, a configuration previously employed for flux-noise suppression in tunable transmons [31–33], protected readout [34–37], and scalable junction fabrication [38]. Under suitable approximations, this element exhibits an effective energy-phase relation analogous to that of a single-channel SNS junction, resulting in a nonsinusoidal potential governed by the junction asymmetry [39]. Experiments conducted on InAs/Al hybrid heterostructures further demonstrate that tuning the junction asymmetry through gate tuning can modify the energy-phase relation from a sinusoidal form to one that closely resembles the SNS junction [40].

In this Letter, we introduce a tunable SIS-SIS circuit element comprising a superconducting quantum

*Contact author: ksenia.shagalov@nbi.ku.dk

†Contact author: mkjaergaard@nbi.ku.dk

Published by the American Physical Society under the terms of the Creative Commons Attribution 4.0 International license. Further distribution of this work must maintain attribution to the author(s) and the published article's title, journal citation, and DOI.

interference device (SQUID) [41,42] in series with a single JJ, enabling *in situ* control of the energy-phase relation via an external magnetic flux, Φ_e, and suitable for integration into a broad range of superconducting circuits. We implement this element as a tunable double-junction transmon, shunted by a large capacitor and operated in the transmon regime. Spectroscopy of higher-order qubit transitions shows an enhanced higher harmonic contribution compared to previously reported values in SIS junctions [3–6]. A model including an auxiliary (internal) mode, associated with the superconducting island between the JJ and SQUID, captures the spectrum and accounts for a renormalization of the qubit frequency. We further observe dispersive coupling of this internal mode to the readout resonator, leading to a flux point where the total ground-state dispersive shift cancels.

Figure 1(a) shows a circuit diagram of the tunable double-junction transmon, with the scanning electron microscope (SEM) images of the corresponding fabricated device shown in Figs. 1(b) and 1(c) (fabrication details can be found in Supplemental Material [43]). We denote by ϕ_1 and ϕ_2 the superconducting phases across the single junction and the SQUID, respectively. To understand the origin of the appreciably higher harmonics in an SIS-SIS device, we consider a "reduced" model in which the charging energy of the middle island is initially omitted. In this limit, the two junctions behave as a single effective element with a potential of the following form [39]:

$$U^{\text{red.}}_{\boxtimes\boxtimes}(\phi_q) = -E_{J\Sigma}\sqrt{1-\lambda\sin^2(\phi_q/2)}, \tag{2}$$

where $\phi_q = \phi_1 + \phi_2$ is the phase of the qubit mode, $E_{J\Sigma} = E_{J1} + E_{J2}$, and

$$\lambda = 4E_{J1}E_{J2}/(E_{J1}+E_{J2})^2 \tag{3}$$

is the junction asymmetry parameter. The resulting potential landscape in this reduced model is shown in Fig. 1(d). The emergence of higher harmonics becomes explicit in the symmetric case $E_{J1} = E_{J2}$, where $\lambda = 1$ and Eq. (2) expands to

$$U^{\text{red.}}_{\boxtimes\boxtimes}(\phi_q) = E_{J\Sigma}\sum_k \left[(-1)^{k+1}\frac{4}{\pi - 4\pi k^2}\right]\cos(k\phi_q), \tag{4}$$

identifying the coefficients in brackets with U_k from Eq. (1). Figure 1(e) shows that the second harmonic can reach $|U_2/U_1| \approx 0.2$ at $\lambda = 1$ [44], substantially larger than previously reported values for single SIS junctions [3–6]. Conversely, for $\lambda \ll 1$, the familiar sinusoidal form is recovered: $U^{\text{red.}}_{\boxtimes\boxtimes}(\phi_q) \propto \cos\phi_q$. Figure 1(f) shows how λ varies with E_{J1}/E_{J2}, reflecting its role as the junction asymmetry parameter, analogous to the effective transmission τ of a single Andreev mode in the SNS potential

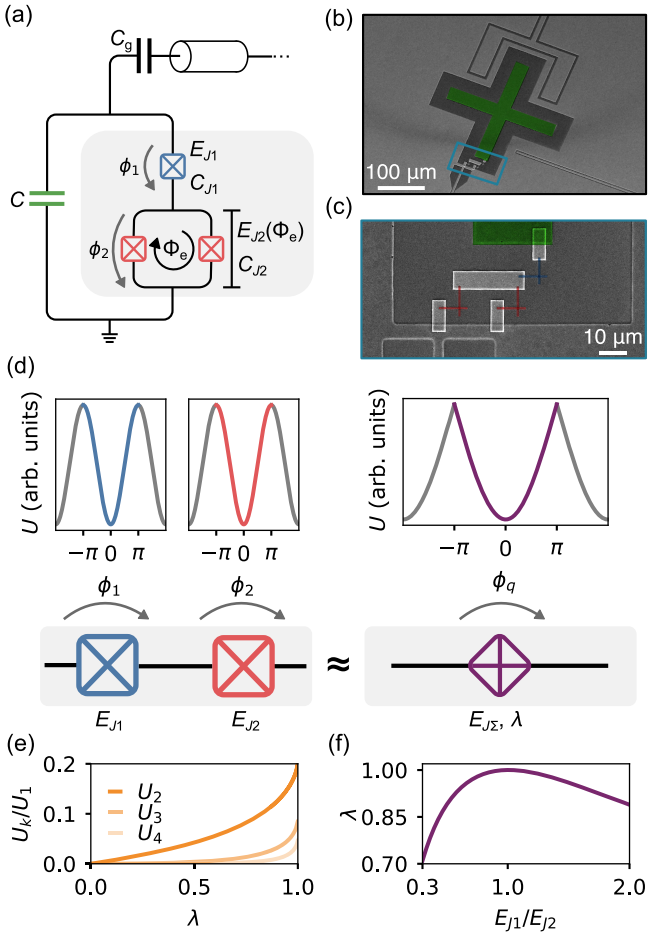


FIG. 1. Qubit circuit and device design. (a) Circuit schematic of the tunable double-junction transmon with a single JJ (blue) and a SQUID loop (red) in series, shunted by a large capacitor (green). (b) SEM of the tunable double-junction transmon showing the large island that forms the capacitor (green). A quarter-wave resonator is capacitively coupled to the qubit for readout. A flux line threads magnetic flux through the SQUID loop, and the drive line facilitates the XY control. (c) SEM image of the single JJ (blue) and the SQUID loop (red) in series. (d) The potentials U plotted for each SIS junction (blue, red), which in series effectively correspond to the potential from Eq. (2), shown for $\lambda = 1$ (purple). (e) Harmonic content of the potential from Eq. (2) as a function of λ. (f) λ as a function of the ratio between the Josephson energies of the two junctions.

$U_{\text{SNS}}(\phi) = -\Delta\sqrt{1-\tau\sin^2(\phi/2)}$, where Δ is the superconducting gap [45].

In the tunable double-junction transmon, threading the external flux through the SQUID loop makes the junction asymmetry parameter flux dependent, $\lambda \to \lambda(\Phi_e)$ and, thereby, allows *in situ* control of the effective potential and its harmonic content. As Fig. 1(f) shows, λ varies slowly near $E_{J1}/E_{J2} \approx 1$, so precise flux biasing to the symmetric point is not required for higher harmonics to be appreciable. In practice, whenever $E_{J2}(\Phi_e)$ lies within roughly a factor of 2 of E_{J1}, the asymmetry parameter

remains above $\lambda \approx 0.9$, corresponding to a second-harmonic ratio of $|U_2/U_1| \approx 0.12$.

In Fig. 2(a), we show the first four transitions of the tunable double-junction transmon as a function of flux threading the SQUID loop. We observe through two-tone spectroscopy the single-photon f_{01} transition together with the multiphoton transitions $f_{02}/2$, $f_{03}/3$, and $f_{04}/4$, from which the higher transition frequencies were extracted through Lorentzian fitting. To fit the spectra as a function of external flux, we use a two-mode Hamiltonian that includes both phase degrees of freedom across the single junction and the SQUID,

$$H_{\text{full}} = 4E_{C1}n_1^2 + 4E_{C2}n_2^2 + g_{12}n_1n_2 + U^{\text{full}}_{\boxtimes\boxtimes}(\phi_1, \phi_2), \tag{5}$$

with

$$U^{\text{full}}_{\boxtimes\boxtimes}(\phi_1, \phi_2) = -E_{J1}\cos(\phi_1) - E_{J2}\cos(\phi_2), \tag{6}$$

where E_{C1}, E_{C2} are the charging energy of each of the modes, n_1, n_2 are their corresponding charge operators, and g_{12} is the coupling between them. We perform a simultaneous fit to all measured f_{01} and $f_{02}/2$ values, extracting the island capacitance as well as the capacitances and Josephson energies of the individual junctions. The resulting fit [solid line in Fig. 2(a)] also accurately predicts f_{03} and f_{04} (dotted gray lines), demonstrating quantitative agreement with the measured spectrum. Details of the circuit model and fitting procedure are provided in Supplemental Material [43].

In Fig. 2(b), we extract the flux-dependent anharmonicity via $\alpha = 2(f_{02}/2 - f_{01})$, shown as green circles. The solid line is the anharmonicity obtained from the fit in Fig. 2(a), again demonstrating good agreement between the two-mode model and the measured spectra. The scatter of the anharmonicity data, on the order of several MHz, is consistent with the uncertainty from Lorentzian fits and may reflect temporal frequency fluctuations typical of superconducting devices. Despite similar configurations being previously employed as weakly flux-tunable transmons [31–33], the tunable double-junction transmon exhibits a pronounced nonmonotonic flux dependence of the anharmonicity between $\Phi_e = 0$ and $\Phi_e = 0.5\Phi_0$. This behavior differs fundamentally from a conventional transmon, where the anharmonicity varies monotonically with flux. The inset of Fig. 2(b) illustrates this comparison using a standard transmon model with identical charging energy, E_C, and matched frequency tunability. Notably, at $\Phi_e = 0$, the tunable double-junction transmon reaches $h\alpha \approx -E_C/3$ [Fig. 2(b)], deviating significantly from the typical transmon value $h\alpha \approx -E_C$ [46].

The qualitative difference between the anharmonicity of the tunable double-junction transmon and that of a conventional transmon can be understood from the reduced model of Eq. (2). Using the reduced potential, the Hamiltonian of the qubit mode is

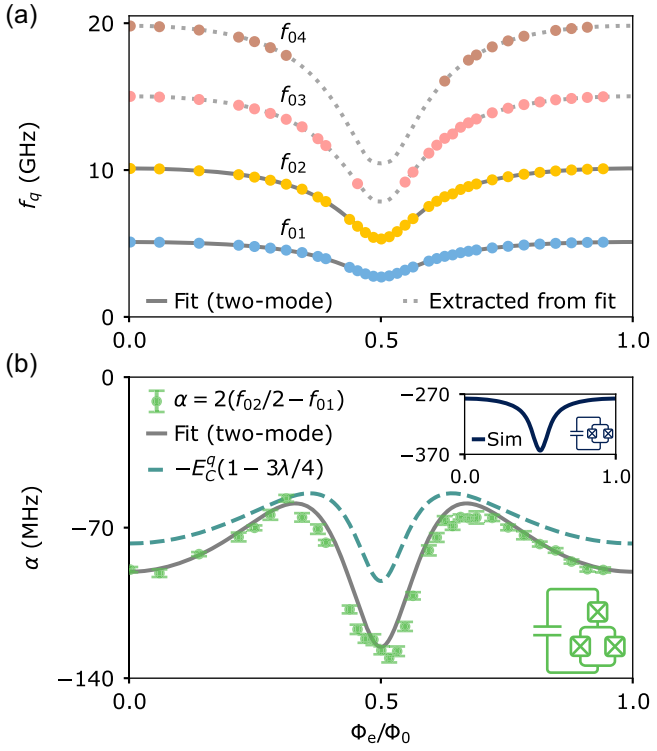


FIG. 2. Flux-dependent two-tone spectroscopy of the tunable double-junction transmon (second cooldown) and fit using the two-mode model from Eq. (5). (a) Two-tone spectroscopy of the f_{01} (light blue), f_{02} (yellow), f_{03} (pink), and f_{04} (brown) transitions as a function of Φ_e. The f_{01} and f_{02} transitions are fitted to the two-mode model of Eq. (5) (solid gray), and the resulting parameters are used to predict f_{03} and f_{04} (dotted gray). (b) Extracted anharmonicity (green) obtained from the f_{01} and $f_{02}/2$ transitions, together with the corresponding fit (solid gray). Error bars indicate the statistical uncertainty extracted from the Lorentzian fits. The analytical expression from Eq. (8), based on the potential in Eq. (2), is shown for comparison (dashed teal). Inset: simulated anharmonicity versus flux for a tunable transmon with comparable device parameters.

$$H_{\text{red.}} = 4E_C^q n_q^2 + U^{\text{red.}}_{\boxtimes\boxtimes}(\phi_q), \tag{7}$$

where $E_C^q = e^2/\{2[C + C_{J1}C_{J2}/(C_{J1} + C_{J2})]\}$ is the charging energy of the qubit mode. Applying the transmon approximation ($E_J^{\text{eff}}/E_C^q \gg 1$) and expanding $U^{\text{red.}}_{\boxtimes\boxtimes}(\phi_q)$ to fourth order yields $hf_{01} \approx \sqrt{8E_C^q E_J^{\text{eff}}} - h\alpha$, with $E_J^{\text{eff}} = E_{J1}E_{J2}/(E_{J1} + E_{J2})$, and an anharmonicity,

$$h\alpha \approx -E_C^q\left(1 - \frac{3}{4}\lambda\right), \tag{8}$$

a result previously demonstrated from studying anharmonicity in gatemons [47]. Figure 2(b) shows Eq. (8) (teal dashed line) evaluated using parameters extracted from the

two-mode fit. The remaining discrepancy between Eq. (8) and the measured anharmonicity arises from the limitations of the transmon approximation and from the internal mode, which renormalizes the qubit spectrum.

We now investigate the presence of higher harmonics in the tunable double-junction transmon. In the two-mode model [Eq. (5)], each junction is described by a sinusoidal potential; thus, higher harmonic content of the qubit mode ϕ_q is not well defined. It emerges only after eliminating the internal degree of freedom and projecting onto an effective single-mode picture, analogous to the emergence of an effective linear inductance in junction-array superinductors [48,49]. The reduced model [Eq. (7)] captures this emergence qualitatively but does not accurately reproduce the measured spectra (see Supplemental Material [43]). To reliably assess the higher harmonic content, we, therefore, derive an approximate single-mode model that incorporates the leading-order effect of the internal mode.

In the situation where the excitations in the internal mode are higher in frequency than the first few qubit excitations, we can apply a Born-Oppenheimer (BO) approximation to describe the low-energy spectrum of the qubit [50,51]. In this approximation, the ground-state energy of the internal mode depends parametrically on ϕ_q and, therefore, acts as an effective potential for the qubit mode. Within an analytical BO approximation framework, we can utilize the fact that the internal mode is transmonlike, i.e., $E_C^{\mathrm{int}}/E_{J\Sigma} \ll 1$, resulting in a BO correction due to the internal mode, up to first order in $E_C^{\mathrm{int}}/E_{J\Sigma}$, given by [44]

$$U_{\boxtimes\boxtimes}^{\mathrm{BO}}(\phi_q) = E_{J\Sigma}\sqrt{\frac{2E_C^{\mathrm{int}}}{E_{J\Sigma}}}\sqrt{1-\lambda\sin^2(\phi_q/2)}, \quad (9)$$

where $E_C^{\mathrm{int}} = e^2/[2(C_{J1}+C_{J2})]$ is the charging energy of the internal mode and $E_C^{\mathrm{int}}/E_{J\Sigma} \sim 1/300$ for our experimental parameters. Thus, our one-dimensional BO model for the qubit mode is given by

$$H_{\mathrm{BO}} = 4E_C^q n_q^2 + U_{\boxtimes\boxtimes}^{\mathrm{red.}}(\phi_q) + U_{\boxtimes\boxtimes}^{\mathrm{BO}}(\phi_q). \quad (10)$$

The harmonic content of this BO model can be extracted via

$$U_k = \frac{1}{\pi}\int_{-\pi}^{\pi}\left[U_{\boxtimes\boxtimes}^{\mathrm{red.}}(\phi_q) + U_{\boxtimes\boxtimes}^{\mathrm{BO}}(\phi_q)\right]\cos(k\phi_q)d\phi_q. \quad (11)$$

In Fig. 3(a), we compare the anharmonicity predicted by the BO model (blue solid line) using the fit parameters extracted from the two-mode model, with the measured values (green points) and find excellent agreement. We extract the junction asymmetry parameter, λ, across flux [Fig. 3(b)], which determines the magnitude of the higher harmonics [Fig. 3(c)]. While junction asymmetry in the SQUID reduces the accessible tuning range of λ, it does not qualitatively alter the emergence of higher harmonics. Figure 3(d) shows a representative spectroscopy measurement at $\Phi_e = 0$, averaged over drive amplitudes, resulting in power broadening of the f_{01} transition. The data are fitted with Lorentzians (solid lines) and compared to BO predictions based on the two-mode model fit parameters (dashed lines), again showing excellent agreement. Using Eq. (11), we extract the first four harmonic coefficients $U_k = [1, 0.107, 0.023, 0.006]$ at $\lambda = 0.85$, in quantitative agreement with Fig. 1(e) and significantly exceeding values reported for single SIS junctions [3–6].

Despite accurately capturing the anharmonicity across all flux values, the BO model fails to reproduce the transition frequencies at $\Phi_e = 0.25\Phi_0$ [Fig. 3(e), dashed lines], due to the strong asymmetry between junction

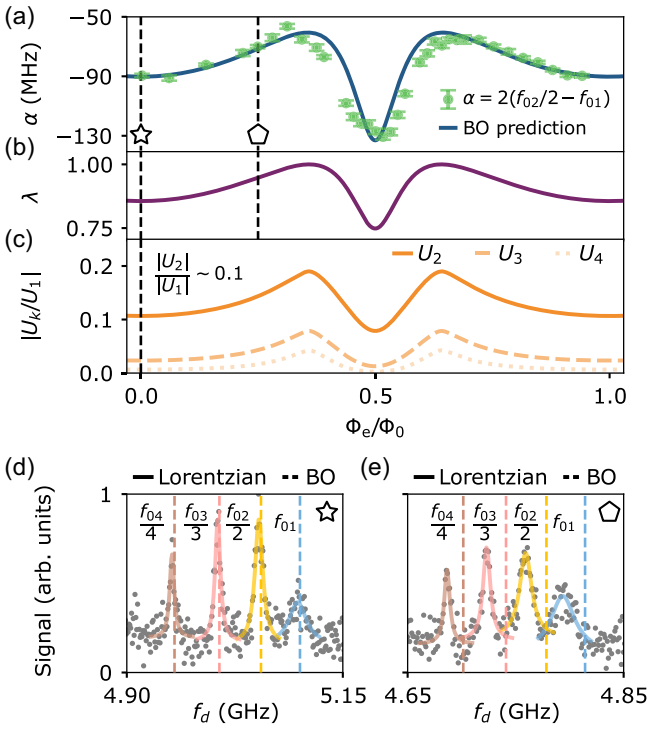


FIG. 3. Measured anharmonicity as a function of flux and extracted harmonic content of the tunable double-junction transmon (second cooldown). (a) Measured anharmonicity values with error bars (green) compared with the Born-Oppenheimer (BO) prediction (blue) using the fit parameters extracted from the two-mode model. Vertical dashed lines mark $\Phi_e = 0$ and $\Phi_e = 0.25\Phi_0$. (b) Extracted junction asymmetry parameter, λ. Vertical dashed lines mark $\lambda = 0.85$ and $\lambda = 0.95$. (c) Extracted second, third, and fourth harmonics normalized to the first harmonic from the BO model; at $\Phi_e = 0$, we obtain $U_k = [1, 0.107, 0.023, 0.006]$. (d) Four observed transitions at $\Phi_e = 0$ with Lorentzian fits (solid) and BO-predicted frequencies (dashed), showing good agreement. (e) Four observed transitions at $\Phi_e = 0.25\Phi_0$; here, the BO model captures the relative level spacings (anharmonicity) but not the absolute transition frequencies.

energies ($E_{J2} < E_{J1}$) and capacitances ($C_{J1} < C_{J2}$) around $\Phi_e = 0.44\Phi_0$. In contrast, the two-mode model remains valid and accurately reproduces the transition frequencies. Extending it to include dispersive coupling to the resonator further provides access to the internal-mode dynamics (see Supplemental Material [43]).

We measure the resonator frequency with the qubit in its ground state as a function of flux [red points in Fig. 4(a)], f_{res}, and fit it simultaneously with f_{01} using the extended two-mode model, thereby extracting the internal-mode frequency (purple) and the coupling to the resonator. Since the qubit transition remains below the bare resonator frequency at 6.378 GHz (red dashed line), the qubit mode alone would produce a positive dispersive shift. In the tunable double-junction transmon, however, the measured ground-state dispersive shift, χ_0, arises from the combined contributions of the qubit and the internal mode,

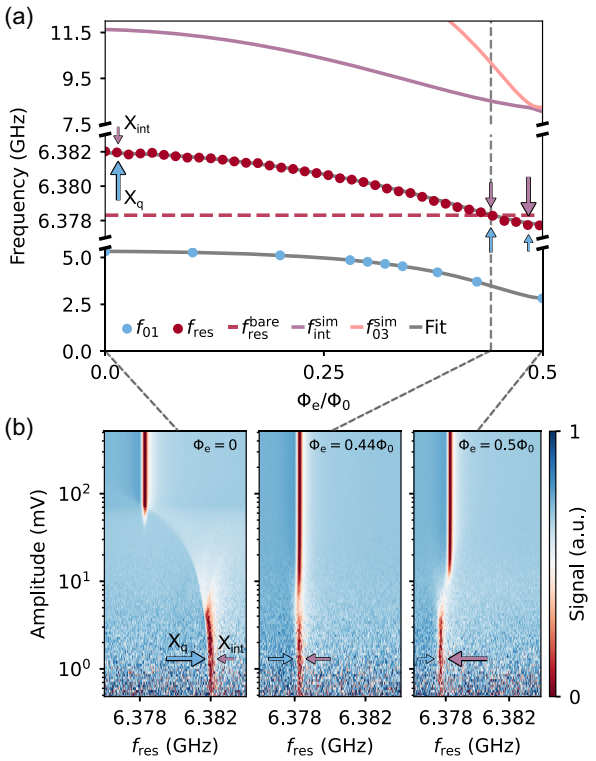


FIG. 4. Flux dependence of the total dispersive shift in the tunable double-junction transmon (first cooldown). (a) Measured data points of the qubit f_{01} (light blue) and of the resonator f_{res} (dark red) with the bare frequency of the resonator $f_{\mathrm{res}}^{\mathrm{bare}}$ indicated by the red dashed line. Extending the two-mode model from Eq. (5) (see Supplemental Material [43]), we fit f_{res} (gray) and extract the simulated internal-mode frequency $f_{\mathrm{int}}^{\mathrm{sim}}$ (purple) and the qubit's f_{03}^{sim} transition, revealing an avoided crossing near $\Phi_e = 0.5\Phi_0$. (b) Resonator spectroscopy versus readout amplitude at three representative flux points. At $\Phi_e = 0$ (left), the qubit contribution dominates, shifting the resonator upward. At the balance point (middle), the qubit and internal-mode contributions cancel, giving zero net dispersive shift. Near $\Phi_e = 0.5\Phi_0$ (right), the internal mode dominates, shifting the resonator downward.

$\chi_0 = \chi_q + \chi_{\mathrm{int}}$. At $\Phi_e = 0$, χ_q dominates, yielding an upward shift [Fig. 4(b), left]; at $\Phi_e = 0.44\Phi_0$, the contributions cancel, giving $\chi_0 = 0$ (middle); and near $\Phi_e = 0.5\Phi_0$, the internal mode dominates, producing a downward shift (right). The flux tunability of χ_0, and in particular the observation of $\chi_0 = 0$, motivates exploration of regimes where the qubit-state-dependent dispersive shift, $\chi_{01} = \chi_1 - \chi_0$, is suppressed, which may be exploited for next-generation qubit readout, particularly when combined with a flux sweet-spot [52–57].

In summary, we have realized and characterized a tunable double-junction transmon composed of a SQUID in series with a single SIS junction, enabling *in situ* flux control of the energy-phase relation. We identified flux regimes where the circuit behaves as a single effective mode and extracted substantially higher harmonic content, including a second harmonic exceeding previously reported values for individual SIS junctions. The internal mode associated with the middle-island charging energy both renormalizes the qubit spectrum, captured in part by a Born-Oppenheimer correction, and couples dispersively to the readout resonator. Due to its large energy separation from the qubit mode and the absence of a direct drive matrix element coupling the two modes, leakage is suppressed. Moreover, as the internal mode resides in the transmon regime, charge dispersion is reduced, and it is, therefore, not expected to introduce significant additional decoherence. Flux-dependent resonator spectroscopy further reveals a balance point where the ground-state dispersive shifts from the qubit and internal modes cancel, yielding a vanishing net shift. These results establish the tunable SIS-SIS element as a building block for superconducting circuits, operating analogously to a conventional SQUID while providing access to higher harmonics within a fully superconducting framework. This enables routes toward protected-qubit designs such as the $\cos(2\phi)$ qubit, which require suppression of the fundamental harmonic, e.g., via interference in a SQUID geometry using multiple SIS-SIS elements [58] or hybrid combinations with SNS junctions [59].

Acknowledgments—We gratefully acknowledge useful discussions with Valla Fatemi, Christian Andersen, Nataliia Zhurbina, and Tyra Cortinez Samenius. This research was supported by the Novo Nordisk Foundation (Grant No. NNF22SA0081175), the NNF Quantum Computing Programme (NQCP), Villum Foundation through a Villum Young Investigator grant (Grant No. 37467), the Innovation Fund Denmark (Grant No. 2081-00013B, DanQ), the U.S. Army Research Office (Grant No. W911NF-22-1-0042, NHyDTech), the European Union through an ERC Starting Grant (Grant No. 101077479, NovADePro), and the Carlsberg Foundation (Grant No. CF21-0343). C. A. P. acknowledges the support of the Natural Sciences and Engineering Research Council of Canada (NSERC)

(No. RGPIN-2026-05057). Finally, we gratefully acknowledge Lena Jacobsen for program management support.

Any opinions, findings, conclusions, or recommendations expressed in this material are those of the author(s) and do not necessarily reflect the views of Army Research Office or the U.S. Government. Views and opinions expressed are those of the author(s) only and do not necessarily reflect those of the European Union or the European Research Council. Neither the European Union nor the granting authority can be held responsible for them.

Data availability—The data that support the findings of this article are openly available [60].

[1] A. Blais, A. L. Grimsmo, S. M. Girvin, and A. Wallraff, Circuit quantum electrodynamics, Rev. Mod. Phys. **93**, 025005 (2021).
[2] B. Josephson, Possible new effects in superconductive tunnelling, Phys. Lett. **1**, 251 (1962).
[3] D. Willsch *et al.*, Observation of Josephson harmonics in tunnel junctions, Nat. Phys. **20**, 815 (2024).
[4] J. Kim, M. Hays, I. T. Rosen, J. An, H. Zhang, A. Goswami, K. Azar, J. M. Gertler, B. M. Niedzielski, M. E. Schwartz, T. P. Orlando, J. A. Grover, K. Serniak, and W. D. Oliver, Emergent harmonics in Josephson tunnel junctions due to series inductance, arXiv:2507.08171.
[5] Z. Wang, R. W. Parker, E. Champion, and M. S. Blok, High-E_J/E_C transmon qudits with up to 12 levels, Phys. Rev. Appl. **23**, 034046 (2025).
[6] M. Féchant, M. F. Dumas, D. Bénâtre, N. Gosling, P. Lenhard, M. Spiecker, S. Geisert, S. Ihssen, W. Wernsdorfer, B. D'Anjou, A. Blais, and I. M. Pop, Offset charge dependence of measurement-induced transitions in transmons, Phys. Rev. Lett. **135**, 180603 (2025).
[7] A. A. Golubov, M. Y. Kupriyanov, and E. Il'ichev, The current-phase relation in Josephson junctions, Rev. Mod. Phys. **76**, 411 (2004).
[8] M. T. Bell, J. Paramanandam, L. B. Ioffe, and M. E. Gershenson, Protected Josephson rhombus chains, Phys. Rev. Lett. **112**, 167001 (2014).
[9] T. W. Larsen, M. E. Gershenson, L. Casparis, A. Kringhøj, N. J. Pearson, R. P. G. McNeil, F. Kuemmeth, P. Krogstrup, K. D. Petersson, and C. M. Marcus, Parity-protected superconductor-semiconductor qubit, Phys. Rev. Lett. **125**, 056801 (2020).
[10] A. Gyenis, A. Di Paolo, J. Koch, A. Blais, A. A. Houck, and D. I. Schuster, Moving beyond the transmon: Noise-protected superconducting quantum circuits, PRX Quantum **2**, 030101 (2021).
[11] C. Schrade, C. M. Marcus, and A. Gyenis, Protected hybrid superconducting qubit in an array of gate-tunable Josephson interferometers, PRX Quantum **3**, 030303 (2022).
[12] L. Banszerus, C. W. Andersson, W. Marshall, T. Lindemann, M. J. Manfra, C. M. Marcus, and S. Vaitiekėnas, Hybrid Josephson rhombus: A superconducting element with tailored current-phase relation, Phys. Rev. X **15**, 011021 (2025).
[13] L. B. Nguyen, H. Kim, D. T. Le, T. Ersevim, S. P. Chitta, T. Chistolini, C. Jünger, W. C. Smith, T. M. Stace, J. Koch, D. I. Santiago, and I. Siddiqi, The superconducting grid-states qubit, arXiv:2509.14656.
[14] A. Gyenis, P. S. Mundada, A. Di Paolo, T. M. Hazard, X. You, D. I. Schuster, J. Koch, A. Blais, and A. A. Houck, Experimental realization of a protected superconducting circuit derived from the $0-\pi$ qubit, PRX Quantum **2**, 010339 (2021).
[15] S. Messelot, A. Leblanc, J. S. Tettekpoe, F. Lefloch, Q. Ficheux, J. Renard, and E. Dumur, Coherence limits in interference-based $\cos(2\varphi)$ qubits, arXiv:2601.10209.
[16] R. S. Souto, M. Leijnse, and C. Schrade, Josephson diode effect in supercurrent interferometers, Phys. Rev. Lett. **129**, 267702 (2022).
[17] C. Ciaccia, R. Haller, Asbjorn C. C. Drachmann, T. Lindemann, M. J. Manfra, C. Schrade, and C. Schönenberger, Gate-tunable Josephson diode in proximitized InAs supercurrent interferometers, Phys. Rev. Res. **5**, 033131 (2023).
[18] S. Reinhardt, T. Ascherl, A. Costa, J. Berger, S. Gronin, G. C. Gardner, T. Lindemann, M. J. Manfra, J. Fabian, D. Kochan, C. Strunk, and N. Paradiso, Link between supercurrent diode and anomalous Josephson effect revealed by gate-controlled interferometry, Nat. Commun. **15**, 4413 (2024).
[19] W. Gibbons, T. Zhang, K. Barrow, T. Lindemann, J. I. Väyrynen, and M. J. Manfra, High efficiency superconducting diode effect in a gate-tunable double-loop squid, arXiv:2512.14909.
[20] C. Ishii, Josephson currents through junctions with normal metal barriers, Prog. Theor. Phys. **44**, 1525 (1970).
[21] Y.-J. Doh, J. A. van Dam, A. L. Roest, E. P. A. M. Bakkers, L. P. Kouwenhoven, and S. De Franceschi, Tunable supercurrent through semiconductor nanowires, Science **309**, 272 (2005).
[22] M. F. Goffman, C. Urbina, H. Pothier, J. Nygård, C. M. Marcus, and P. Krogstrup, Conduction channels of an InAs-Al nanowire Josephson weak link, New J. Phys. **19**, 092002 (2017).
[23] A. Maiani, K. Flensberg, M. Leijnse, C. Schrade, S. Vaitiekėnas, and R. Seoane Souto, Nonsinusoidal current-phase relations in semiconductor–superconductor–ferromagnetic insulator devices, Phys. Rev. B **107**, 245415 (2023).
[24] E. M. Spanton, M. Deng, S. Vaitiekėnas, P. Krogstrup, J. Nygård, C. M. Marcus, and K. A. Moler, Current–phase relations of few-mode InAs nanowire Josephson junctions, Nat. Phys. **13**, 1177 (2017).
[25] T. W. Larsen, K. D. Petersson, F. Kuemmeth, T. S. Jespersen, P. Krogstrup, J. Nygård, and C. M. Marcus, Semiconductor-nanowire-based superconducting qubit, Phys. Rev. Lett. **115**, 127001 (2015).
[26] G. de Lange, B. van Heck, A. Bruno, D. J. van Woerkom, A. Geresdi, S. R. Plissard, E. P. A. M. Bakkers, A. R. Akhmerov, and L. DiCarlo, Realization of microwave quantum circuits using hybrid superconducting-semiconducting nanowire Josephson elements, Phys. Rev. Lett. **115**, 127002 (2015).
[27] S. Liu, A. Bordoloi, J. Issokson, I. Levy, M. G. Vavilov, J. Shabani, and V. E. Manucharyan, Strongly anharmonic

flux-tunable transmon based on InAs-Al 2D heterostructure, Nat. Commun. **17**, 740 (2025).
[28] B. Zhang, Z. Li, V. Aguilar, P. Zhang, M. Pendharkar, C. P. Dempsey, J. S. Lee, S. D. Harrington, S. Tan, J. S. Meyer, M. Houzet, C. J. Palmstrøm, and S. M. Frolov, Evidence of ϕ_0-Josephson junction from skewed diffraction patterns in Sn-InSb nanowires, SciPost Phys. **18**, 013 (2025).
[29] D. Feldstein-Bofill, Z. Sun, C. Wied, S. Singh, B. D. Isakov, S. Krøjer, J. Hastrup, A. Gyenis, and M. Kjaergaard, Gatemon qubit revisited for improved reliability and stability, Phys. Rev. Appl. **24**, 044099 (2025).
[30] Z. Sun, D. Feldstein-Bofill, K. Shagalov, A. T. J. Paulsen, C. Wied, S. Singh, B. D. Isakov, J. Hastrup, C. W. Warren, S. Krøjer, A. Kringhøj, A. Gyenis, and M. Kjaergaard, Junction-intrinsic dissipation in hybrid superconductor-semiconductor gatemon qubits, arXiv:2603.29498.
[31] J. M. Chávez-Garcia, F. Solgun, J. B. Hertzberg, O. Jinka, M. Brink, and B. Abdo, Weakly flux-tunable superconducting qubit, Phys. Rev. Appl. **18**, 034057 (2022).
[32] E. Y. Egorova, A. S. Kazmina, and I. N. Moskalenko, A weakly-tunable transmon qubit with an optimized shape of the shunted capacitance, Pis'ma Zh. Tekh. Fiz. **50**, 10 (2024).
[33] E. Y. Egorova, A. S. Kazmina, I. A. Simakov, I. N. Moskalenko, N. N. Abramov, D. A. Kalacheva, V. B. Lubsanov, A. N. Bolgar, N. Maleeva, and I. S. Besedin, Three-mode tunable coupler for superconducting two-qubit gates, arXiv:2405.10886.
[34] J. Hu, A. L. R. Manesco, A. Melo, T. V. Stefanski, C. K. Andersen, and V. Fatemi, Mixed spin-boson coupling for qubit readout with suppressed residual shot-noise dephasing, arXiv:2503.13411.
[35] S. Hazra, W. Dai, T. Connolly, P. D. Kurilovich, Z. Wang, L. Frunzio, and M. H. Devoret, Benchmarking the readout of a superconducting qubit for repeated measurements, Phys. Rev. Lett. **134**, 100601 (2025).
[36] G. Beaulieu, J.-Z. Chen, M. Scigliuzzo, O. Benhayoune-Khadraoui, A. A. Chapple, P. A. Spring, A. Blais, and P. Scarlino, Fast, high-fidelity transmon readout with intrinsic purcell protection via nonperturbative cross-Kerr coupling, arXiv:2601.04975.
[37] J. B. Kline, A. Yen, S. Chen, and K. P. O'Brien, The arm qubit: A superconducting qubit co-designed for coherence and coupling, arXiv:2506.05315.
[38] P. Sethi, O. Prakash, J.-P. Kaikkonen, M. Kervinen, E. T. Mannila, M. Ribeiro, D. Datta, C. W. Förbom, J. Senior, R. P. Loreto, J. Hätinen, K. Viisanen, J. I. Väyrynen, A. Ronzani, A. Kemppinen, V. Vesterinen, M. Prunnila, and J. Govenius, Native-oxide-passivated trilayer junctions for superconducting qubits, arXiv:2504.03481.
[39] A. M. Bozkurt, J. Brookman, V. Fatemi, and A. R. Akhmerov, Double-Fourier engineering of Josephson energy-phase relationships applied to diodes, SciPost Phys. **15**, 204 (2023).
[40] L. Banszerus, W. Marshall, C. W. Andersson, T. Lindemann, M. J. Manfra, C. M. Marcus, and S. Vaitiekėnas, Voltage-controlled synthesis of higher harmonics in hybrid Josephson junction circuits, Phys. Rev. Lett. **133**, 186303 (2024).
[41] R. C. Jaklevic, J. Lambe, A. H. Silver, and J. E. Mercereau, Quantum interference effects in Josephson tunneling, Phys. Rev. Lett. **12**, 159 (1964).
[42] P. Krantz, M. Kjaergaard, F. Yan, T. P. Orlando, S. Gustavsson, and W. D. Oliver, A quantum engineer's guide to superconducting qubits, Appl. Phys. Rev. **6**, 021318 (2019).
[43] See Supplemental Material at http://link.aps.org/supplemental/10.1103/fr7x-555s for information on the fabrication and measurement setup, data analysis, and theoretical modeling.
[44] L. U. Jakobsen, K. Shagalov, D. Feldstein-Bofill, M. Kjaergaard, K. Flensberg, and S. Krøjer, Low-energy spectrum of double-junction superconducting circuits in the Born-Oppenheimer approximation, arXiv:2603.26374.
[45] C. W. J. Beenakker, Universal limit of critical-current fluctuations in mesoscopic Josephson junctions, Phys. Rev. Lett. **67**, 3836 (1991).
[46] J. Koch, T. M. Yu, J. Gambetta, A. A. Houck, D. I. Schuster, J. Majer, A. Blais, M. H. Devoret, S. M. Girvin, and R. J. Schoelkopf, Charge-insensitive qubit design derived from the Cooper pair box, Phys. Rev. A **76**, 042319 (2007).
[47] A. Kringhøj, L. Casparis, M. Hell, T. W. Larsen, F. Kuemmeth, M. Leijnse, K. Flensberg, P. Krogstrup, J. Nygård, K. D. Petersson, and C. M. Marcus, Anharmonicity of a superconducting qubit with a few-mode Josephson junction, Phys. Rev. B **97**, 060508(R) (2018).
[48] V. E. Manucharyan, J. Koch, L. I. Glazman, and M. H. Devoret, Fluxonium: Single Cooper-pair circuit free of charge offsets, Science **326**, 113 (2009).
[49] A. Di Paolo, T. E. Baker, A. Foley, D. Sénéchal, and A. Blais, Efficient modeling of superconducting quantum circuits with tensor networks, npj Quantum Inf. **7**, 11 (2021).
[50] A. Ciani, D. P. DiVincenzo, and B. M. Terhal, *Lecture Notes on Quantum Electrical Circuits* (TU Delft OPEN Publishing, Delft, NL, 2025), 10.59490/tb.85.
[51] M. Rymarz and D. P. DiVincenzo, Consistent quantization of nearly singular superconducting circuits, Phys. Rev. X **13**, 021017 (2023).
[52] C. Lledó, R. Dassonneville, A. Moulinas, J. Cohen, R. Shillito, A. Bienfait, B. Huard, and A. Blais, Cloaking a qubit in a cavity, Nat. Commun. **14**, 6313 (2023).
[53] M. H. Muñoz Arias, C. Lledó, and A. Blais, Qubit readout enabled by qubit cloaking, Phys. Rev. Appl. **20**, 054013 (2023).
[54] F. Swiadek, R. Shillito, P. Magnard, A. Remm, C. Hellings, N. Lacroix, Q. Ficheux, D. C. Zanuz, G. J. Norris, A. Blais, S. Krinner, and A. Wallraff, Enhancing dispersive readout of superconducting qubits through dynamic control of the dispersive shift: Experiment and theory, PRX Quantum **5**, 040326 (2024).
[55] T. V. Stefanski and C. K. Andersen, Flux-pulse-assisted readout of a fluxonium qubit, Phys. Rev. Appl. **22**, 014079 (2024).
[56] T. V. Stefanski, F. Yilmaz, E. Y. Huang, M. F. S. Zwanenburg, S. Singh, S. Wang, L. J. Splitthoff, and C. K. Andersen, Improved fluxonium readout through dynamic flux pulsing, arXiv:2411.13437.

[57] F. Pfeiffer *et al.*, Efficient decoupling of a nonlinear qubit mode from its environment, Phys. Rev. X **14**, 041007 (2024).

[58] N. K. Zhurbina, S. Singh, L. J. Splitthoff, E. Y. Huang, F. Yilmaz, A. M. Bozkurt, and C. K. Andersen, Coherence limitations of a Fourier-engineered $\cos(2\varphi)$ transmon qubit, arXiv:2605.06372.

[59] D. Feldstein-Bofill, L. U. Jacobsen, K. Shagalov, Z. Sun, C. Wied, S. Singh, A. Kringhøj, J. Hastrup, A. Gyenis, K. Flensberg, S. Krøjer, and M. Kjaergaard, Controlled parity of Cooper pair tunneling in a hybrid superconducting qubit, arXiv:2601.11303.

[60] Data available at Zenodo, https://zenodo.org/records/17957412.